BMC Cancer

RESEARCH

Open Access

Understanding m6A changes in chromophobe renal cell carcinoma and predicting patient outcomes survival

Zhigang Chen[1†], Junbo Yang[2†], Wei Zhang[2†], Yang Qian[2], Nan Zhang[2], Zixin Chen[2], Min Lu[3,4], Liyuan Ge[3], Cheng Liu[3], Xiaojun Tian[3], Guifang Jia[2*], Lulin Ma[3*] and Baoguo Li[1*]

Abstract

N6-methyladenosine (m^6A) is a prevalent mRNA modification known for its implications in various cancer types, yet its role in chromophobe renal cell carcinoma (chRCC) remains largely unexplored. In this study, we performed m6A-SEAL-seq and RNA-seq analyses on tissues from three chRCC subjects, aiming to uncover m^6A alterations in chRCC. Our findings revealed reduced expression levels of four m^6A regulators in chRCC tissues and highlighted differences in m^6A levels compared to normal tissues. Furthermore, we identified specific genes and cancer-related pathways affected by these differences, including notable candidates like NOTCH1 and FGFR1, implicated in chRCC development. Additionally, we developed a predictive model based on the expression level of m^6A associated genes, demonstrating promising prognostic capabilities for patient survival prediction. Overall, our study provides valuable insights into the role of m^6A in chRCC and its potential as a prognostic indicator.

Keywords Chromophobe renal cell carcinoma, N^6-methyladenosine, Transcriptome, Prognostic indicator

Introduction

According to the Global Cancer Observatory (GCO, https://gco.iarc.fr/en) database as of 2022, kidney cancer accounts for over 434 thousand new cases globally, with more than 155 thousand deaths attributed to the disease. Despite advancements in healthcare, kidney cancer remains a significant public health concern, ranking 16th in terms of incidence and 17th in terms of cancer-related mortality worldwide. The urgent need to decipher the molecular mechanisms underlying kidney cancer progression persists.

There are three primary types of kidney cancer: clear cell renal cell carcinoma (ccRCC), papillary renal cell carcinoma (PRCC), and chromophobe renal cell carcinoma (chRCC). Among these, ccRCC is the most prevalent form of kidney cancer. Significant advancements have been made in understanding the pathogenesis and therapeutic approaches for ccRCC [1–4]. Papillary renal cell

†Zhigang Chen, Junbo Yang and Wei Zhang contributed equally to this work.

*Correspondence:
Guifang Jia
guifangjia@pku.edu.cn
Lulin Ma
puth_malulin@163.com
Baoguo Li
libaoguo_hdyy@163.com
[1]Department of Urology, Beijing Haidian Hospital (Haidian Section of Peking University Third Hospital), Beijing 100080, China
[2]Synthetic and Functional Biomolecules Center, Beijing National Laboratory for Molecular Sciences, Key Laboratory of Bioorganic Chemistry and Molecular Engineering of Ministry of Education, College of Chemistry and Molecular Engineering, Peking University, Beijing 100871, China
[3]Department of Urology, Peking University Third Hospital, Beijing 100191, China
[4]Department of Pathology, Peking University Third Hospital, Beijing 100191, China

© The Author(s) 2024. **Open Access** This article is licensed under a Creative Commons Attribution-NonCommercial-NoDerivatives 4.0 International License, which permits any non-commercial use, sharing, distribution and reproduction in any medium or format, as long as you give appropriate credit to the original author(s) and the source, provide a link to the Creative Commons licence, and indicate if you modified the licensed material. You do not have permission under this licence to share adapted material derived from this article or parts of it. The images or other third party material in this article are included in the article's Creative Commons licence, unless indicated otherwise in a credit line to the material. If material is not included in the article's Creative Commons licence and your intended use is not permitted by statutory regulation or exceeds the permitted use, you will need to obtain permission directly from the copyright holder. To view a copy of this licence, visit http://creativecommons.org/licenses/by-nc-nd/4.0/.

carcinoma (PRCC) stands as the second most common type of renal carcinoma and is currently a well-studied subtype of renal cell carcinoma (RCC) [5, 6]. Whereas chRCC is an uncommon renal cell carcinoma (RCC) subtype, accounting for 5–10% of all cases of RCC [7]. Previous studies suggest that chRCC is a malignant neoplasm with a mortality rate of about 10%, and aggressive clinical course such as metastasis [8]. While the somatic genomic landscape of chRCC has revealed various genomic features [9], the understanding of the functional role of epitranscriptomics remains limited.

More than 170 types of modifications have been identified in the RNA molecule [10]. N^6-methyladenine (m^6A) emerges as the most abundant mRNA modification in eukaryotes, playing pivotal roles in various biological functions. These functions include the regulation of RNA stability [11–13], 3′-end processing [14, 15], alternative splicing [16, 17] and translation efficiency at the post-transcriptional level [13, 18, 19]. m^6A is dynamically reversible in mammals and is governed by "writers" (methyltransferases), "erasers" (demethylases), and "readers" (binding proteins). The majority of m^6A modifications are installed by the methyltransferase complex, primarily composed of the METTL3-METTL14 heterodimer [20, 21] and other subunits like WTAP [22–24], and removed by demethylases like FTO and ALKBH5 [25, 26]. m^6A modification can also be recognized and bound by m^6A binding proteins for the regulation of gene expression, like YTH domain family proteins [27–29]. The discovery of these diverse m^6A regulators has significantly contributed to a deeper understanding of the physiological functions of m^6A.

Numerous studies have underscored the close relationship between m6A modifications and tumor progression [30–33]. In pancreatic cancer, ALKBH5 inhibits cancer cell growth and progression by increasing PER1 mRNA levels through m^6A removal, consequently inhibiting YTHDF2-dependent mRNA degradation [33]. In bladder cancer, METTL3 installs m^6A on pri-miR221/222, expediting miRNA maturation and promoting cancer cell proliferation [34]. These findings highlight the pivotal roles of m^6A modification in carcinogenesis through the regulation of RNA processing and metabolism, shedding light on new molecular mechanisms underlying cancer progression. m^6A regulators exert significant impacts on clear cell renal cell carcinoma (ccRCC) [35]. METTL14, for instance, is downregulated in ccRCC tissue, and patients with lower METTL14 expression tend to exhibit worse prognoses [36]. Alterations in m^6A regulators are associated with worse clinical characteristics [37]. In RPCC, a prognostic risk signature model incorporating three m^6A regulatory genes, IGF2BP3, KIAA1429, and HNRNPC, accurately predicts survival outcomes [38]. The advent of high-throughput sequencing has enabled transcriptome-wide profiling of m^6A distribution in various human carcinomas, offering insights into the molecular mechanisms underlying m^6A modification and renal cell carcinoma (RCC). Transcriptome-wide m^6A mapping in ccRCC has revealed the identification of unique m^6A-related genes associated with cancer-related pathways and provided insights into potential mechanisms of m^6A-mediated gene regulation [39]. However, the transcriptome-wide distribution of m^6A in chRCC remains elusive. In this study, we utilized m6A-SEAL-seq to construct a landscape of m^6A profiling in human chRCC [40], and identified novel m^6A gene signature.

Methods

Patients and specimens

A total of three patients with chRCC were involved in our study. chRCC tissues and corresponding tumor-adjacent normal tissues were collected at the time of surgery from urology department, Peking University Third Hospital. All specimens were immediately separated into 1.5 ml RNase-free centrifuge tubes and stored at -80 °C before RNA isolation. The study was approved by The Beijing Haidian Hospital Medical Ethics Committee, and the written informed consents were obtained from all the participants.

RNA preparation

Total RNA was extracted from tissue specimens using TRIzol reagent (Magen) and poly(A)$^+$ RNA was isolated from total RNA using oligo(dT) 25 Dynabeads (Thermo Fisher Scientific). RNA concentration was determined using a Nanodrop ultraviolet-visible light spectrophotometer (Thermo).

qRT–PCR

Poly(A)$^+$ RNA was isolated from tissues using TRIzol reagent (Invitrogen) and oligo(dT)$_{25}$ Dynabeads (Thermo Fisher Scientific). First-strand cDNA synthesis was carried out using SuperScript III (Thermo Fisher Scientific) and oligo(dT)$_{20}$ primer. Each sampling was performed with at least three biological replicates. The relative expression levels were normalized using GADPH as the reference gene. All the primers were designed by multiPrime at https://multiprime.cn [41]. All primer sequences are provided in Supplementary Dataset 1.

m^{6}A-SEAL-seq and library construction

Poly(A)$^+$ RNA for each sample was fragmented by a magnesium RNA fragmentation module (NEB). In a poly(A)$^+$ RNA m^6A oxidation assay, the reaction was performed in 300 µl aliquots of aqueous solution containing 300 µM of $(NH_4)_2Fe(SO_4)_2{\cdot}6H_2O$, 2 mM of l-ascorbic acid, 300 µM of α-KG, 100 mM pH 7.0 HEPES, 0.2 µM FTO and 1 µg poly(A)$^+$ RNA. After the FTO treatment at 37 °C

for 5 min, RNA was purified by Oligo Clean & Concentrator column (Zymo Research). hm^{6}A-modified RNA converted from m^{6}A by FTO oxidation was treated by 200 mM freshly prepared DTT at 37 °C for 3 h in acidic aqueous solution (100 mM HEPES, pH 4.0). The product RNA was purified by ethanol precipitation. After ethanol precipitation, DTT treated RNA was washed by 75% ethanol and dissolved in 200 µl biotinylation buffer that contained 100 µM of MTSEA-XX-biotin (Biotum), 100 mM HEPES (pH 7.0), 1 mM EDTA and 20% DMF. The reaction was performed at 25 °C and 800 rpm in a ThermoMixer for 1 h. The product RNA was purified by phenol-chloroform extraction. 50 ng biotin-labeled RNA was saved as input, and the rest proceeded to affinity enrichment. After that, 20 µl Dynabeads MyOne Streptavidin C1 (Invitrogen) was washed twice by 200 µl 0.1 M NaOH to remove RNase contamination, and then washed with diethyl pyrocarbonate water to a neutral pH. The beads were resuspended in 100 µl binding solution containing 10 µl of high-salt wash buffer (100 mM Tris pH 7.5, 10 mM EDTA, 1 M NaCl, 0.05% Tween 20) and 90 µl diethyl pyrocarbonate water, and incubated with the biotinylated RNA for 1 h. The beads with biotinylated RNA were washed three times with 1 ml high salt wash buffer. 50 µl of 100 mM DTT was used to release the biotinylated RNA at 37 °C for 15 min on a ThermoMixer (800 rpm.). After collecting the supernatant, the second elution was performed with 50 µl of 100 mM DTT at 50 °C for 5 min to completely release the RNA. The twice-eluted RNA was combined and purified by ethanol precipitation. Library construction was performed using NEBNext Ultra II Directional RNA Library Prep Kit for Illumina according to the manufacturer's protocol. Libraries were sequenced on the Illumina HiSeq XTen platform with a paired-end model (PE150).

Analysis of m^{6}A-seq data

Sequencing reads were trimmed and mapped to the reference genome (GRCh38) by using Cutadapt (v1.18) [42] and HISAT2 (v2.1.0) [43], respectively. The m^{6}A-enriched regions in chRCC and normal tissues were identified using the MACS2 [44] peak-calling algorithm based on enrichment criteria (IP/Input)≥2 and FDR<0.05. Confident m^{6}A peaks were subjected to Hypergeometric Optimization of Motif EnRichment tools (HOMER) [45] for Motif Discovery. Genes with differentially methylated m^{6}A sites were identified by MeTDiff [46] based on enrichment criteria fold change≥2 and FDR<0.05. Tissue analysis, Gene ontology (GO) and pathway enrichment analyses were performed by using DAVID.

Analysis of RNA-seq data

Adapter and low-quality reads were trimmed by using Cutadapt (v1.18) [42], and trimmed reads were aligned to the reference genome (GRCh38) using HISAT2 (v2.1.0) [43]. The differential expression genes between chRCC and adjacent normal tissues were screened by R package (DEseq2) [47] based on a cutoff criterion of fold change≥2 and FDR<0.05.

Risk stratification and survival analysis

A cohort of 65 chRCC cases from The Cancer Genome Atlas (TCGA) database was used to illustrate the relationship between the differential expressed DMMGs and chRCC patients. We randomly chose 40 samples from 65 cases as a training set to predict signature model and the rest samples form a testing set to verify the model (make sure the training set and testing set both contain tumor samples and normal samples). Firstly, we used least absolute shrinkage and selection operator (LASSO) to select candidate genes (glmnet package) in training set. Secondly, we performed the multi-variates cox regression and removed genes not supported by PH hypothesis using the selected candidate genes in training set. Thirdly, we performed the second regression (survival package) to calculate the coefficients between candidate genes and 5-years survival using the remaining candidate genes in training set to build a Cox model. The concordance index (C-index) was calculated to evaluate the prognostic power. Risk score of each sample was calculated through the sum of the product of each candidate gene fpkm-uq and its coefficient in training set. The patients were then classified into high-risk or low-risk group using the risk score where the difference value of true positive and false positive reaches to the maximum as the cutoff value. The Kaplan-Meier survival curve (survminer package) was performed to evaluate the 5-years survival, and the sensitivity and accuracy of the cox model to predict clinical outcome were evaluated by the area under curve (AUC) of the receiver operating characteristic (ROC) curve (survival ROC package). At last, we test the signature model in the testing set, ccRCC dataset (a cohort of 602 cases from TCGA database) and PRCC dataset (a cohort of 318 cases from TCGA database).

Results

The expression pattern of m^{6}A regulators in normal and chRCC tissue

In order to determine whether m^{6}A modification functions in chRCC, we first analyzed the expression levels of 8 m^{6}A regulators, including 3 key writer subunits, 3 readers, and 2 erasers (m^{6}A writer subunits: METTLE14, METTL3, and WTAP; m^{6}A readers: YTHDF1, YTHDF2, and YTHDF3; m^{6}A erasers: ALKBH5 and FTO) in three patients. The qPCR results showed that the expression levels of WTAP, YTHDF2, FTO, and ALKBH5 were downregulated markedly in chRCC tissues compared with corresponding tumor-adjacent normal tissues

(termed normal tissues) (Fig. 1A-H). Furthermore, upon comparison with The Cancer Genome Atlas (TCGA database), we observed a notable decrease in the expression of the m^{6}A writer WTAP as well (Fig. S1). The aberrant expression of the m^{6}A regulators in chRCC, suggesting m^{6}A might be dysregulated in chRCC.

Overview of m^{6}A methylation feature in normal and chRCC tissues

To investigate whether m^{6}A methylation landscape changes between the normal and chRCC tissues, we next constructed m^{6}A-SEAL-seq using three samples and explored the distribution of m^{6}A modification [40]. Approximately 87.1–13.2 million reads were generated from each library and 82.8–12.8 million reads were mapped to GRCh38 genome (Supplementary Dataset 2). m^{6}A peaks were called in each sample using MACS2, based on fold enrichment (IP/input) ≥ 2 and FDR ≤ 0.05). The m^{6}A peaks identified in all three replicates were classified as "confident m^{6}A peaks". Finally, we identified 15,024 confident m^{6}A peaks corresponding to 11,396 transcripts/genes in normal tissues, whereas 12,841 confident m^{6}A peaks corresponding to 10,102 transcripts/genes in chRCC tissue (Fig. 2A). To evaluate the reliability and performance of m^{6}A-SEAL-seq, we compared our confident m^{6}A peaks of normal tissues with MeRIP-seq of normal kidney tissues from published sequencing data (GSE122744) [48]. 5686 out of 7261 (78.3%) of the m^{6}A peaks in MeRIP-seq were identified as confident m^{6}A peaks in our m^{6}A-SEAL-seq (Fig. S2A), and the metagene profile results of m^{6}A-SEAL-seq and MeRIP-seq indicated that that our confident m^{6}A peaks were highly enriched around MeRIP-seq peaks (Fig. S2B). We additionally computed normalized read coverages from m^{6}A-SEAL-seq around MeRIP-seq peaks, revealing their co-enrichment (Fig. S2C, D). These findings suggest that m^{6}A-SEAL-seq provides accurate and reliable results.

The metagene profiles results demonstrated that confident m^{6}A peaks in normal and chRCC tissue were both highly located within Coding Sequence (CDS) (Fig. 2B). However, the distribution pattern of m^{6}A peaks in chRCC shifted from CDS region to stop codon and 3'UTR. To further locate confident m^{6}A peaks, we divided the transcripts into five non-overlapping regions and assigned the confident m^{6}A peaks into these regions. The fraction of confident m^{6}A peaks of normal and chRCC tissues (Fig. 2C) in these five regions showed that they were dominantly enriched in 3′ UTR (40.46%, 40.55%), CDS (29.01%, 26.54%) and stop codon (17.32%, 18.59%). The motifs analysis results revealed that in

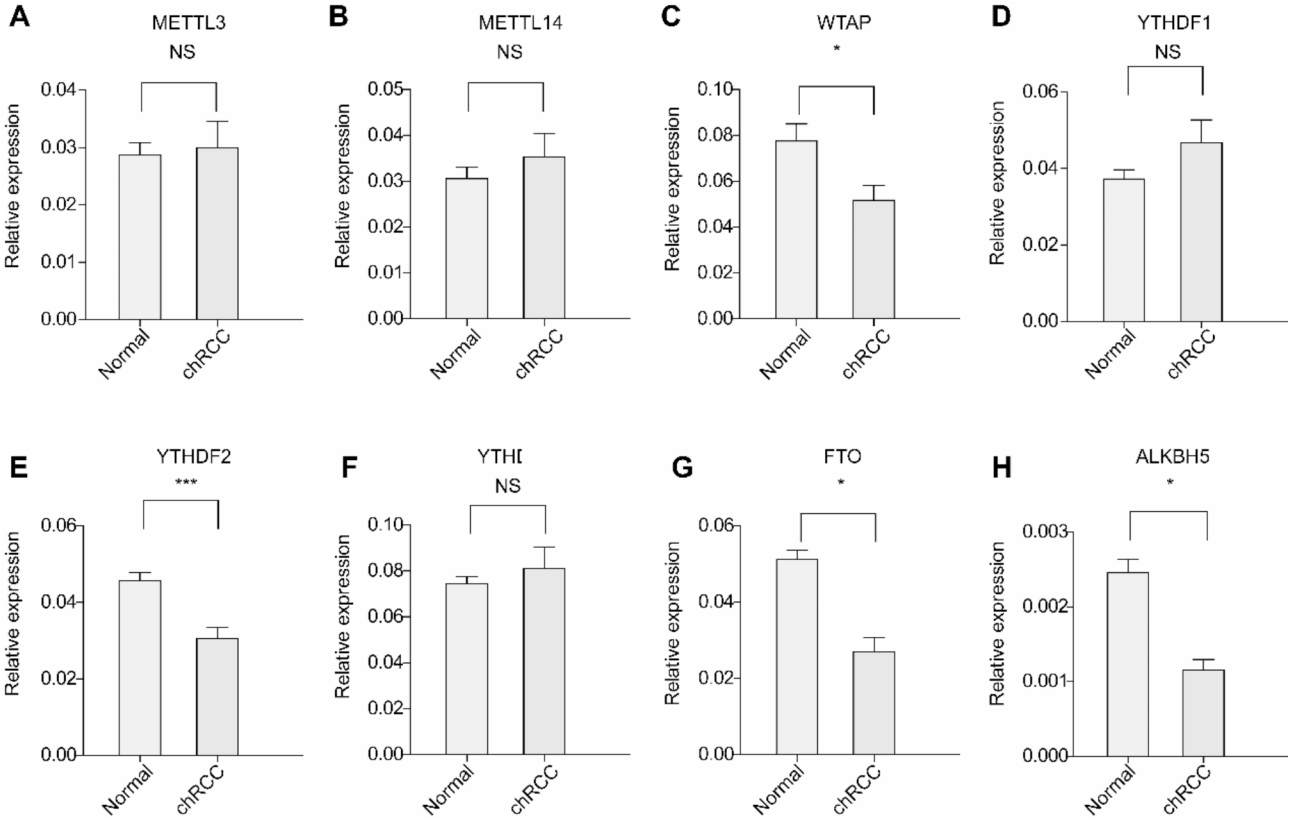

Fig. 1 Relative expression level of known m^{6}A-related genes in Normal and chRCC tissues by qPCR. **A**, METLL3, **B**, METTL14, **C**, WTP, **D**, YTHDF1, **E**, YTHDF2, **F**, YTHDF3, **G**, FTO, **H**, ALKBH5. Data are presented as means ± SE, $n = 3$ biological replicates. *$P < 0.05$ by t test (two-sided)

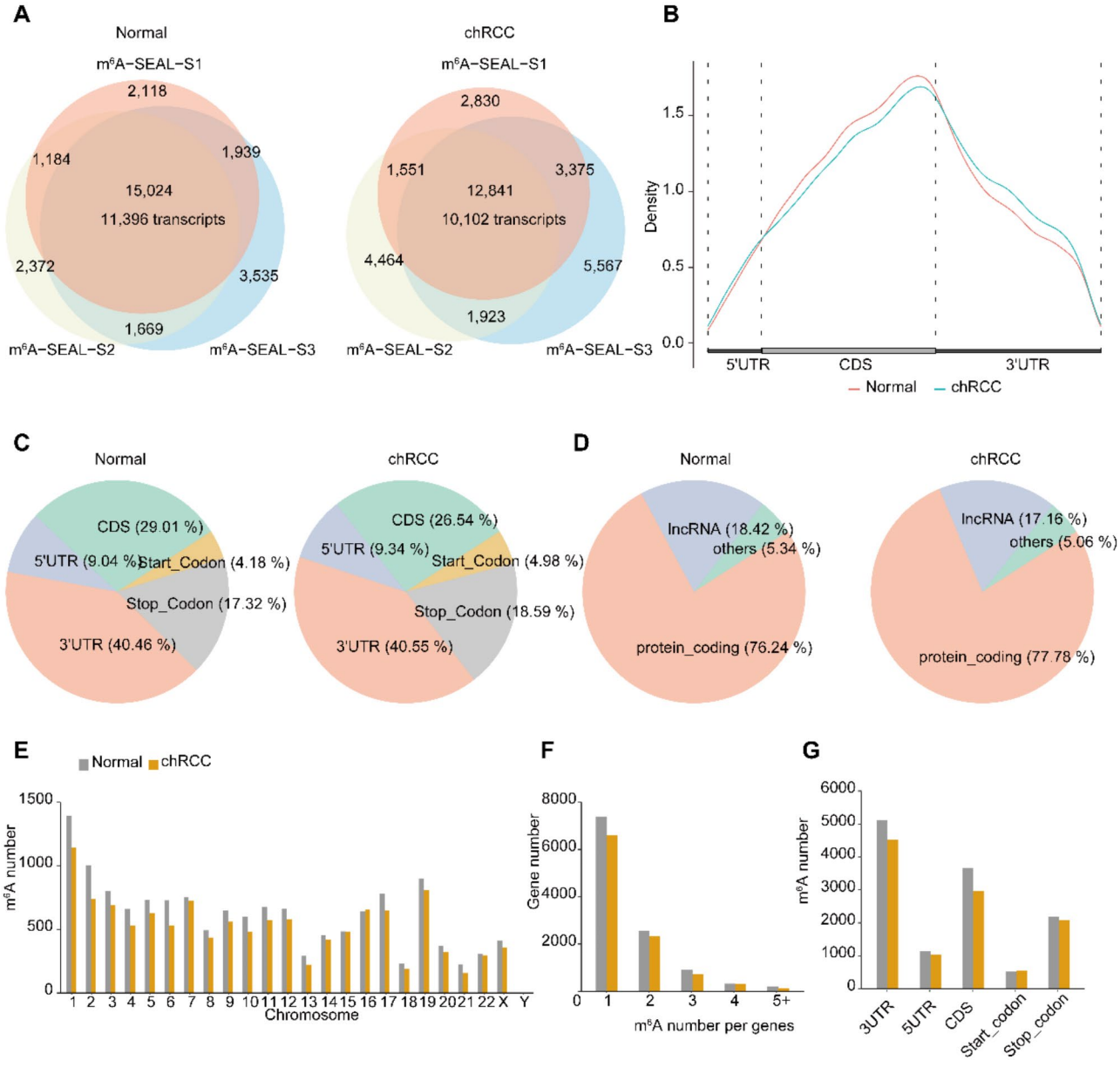

Fig. 2 Characterization of m^6 A modification in Normal and chRCC tissues reveals that decreased methylation number in chRCC Tissues. **A**, overlap of three biological replicates of m^{6}A-SEAL-seq peaks identifying ~ 15,000 high-confident m^{6}A peaks corresponding to 11,396 unique transcripts in normal tissues (left); Overlap of three biological replicates of m^{6}A-seal peaks identifying ~ 12,800 high-confident m^{6}A peaks corresponding to 10,102 unique transcripts in chRCC tissues (right). **B**, Metagene profile illustrating the region distribution of m^{6}A peaks across the indicated mRNA segments. **C**, Pie chart depicting the fraction of the confident m^{6}A peaks in each of the five non-overlapping transcript segments (5'UTR, start codon, coding sequence [CDS], stop codon and 3'UTR) in normal tissues (left); Pie chart depicting RNA types of m^{6}A peaks in normal tissues (right). **D**, Pie chart presenting the fraction of the confident m^{6}A peaks in eCRCC tissues (left); Pie chart depicting RNA types of m^{6}A peaks in chRCC tissues (right). **E**, The number of m^{6}A peaks in human chromosomes. **F**, The number of m^{6}A peaks per gene. **G**, The number of m^{6}A peaks in five non-overlapping transcript segments

both normal and chRCC tissues, the identified motifs are GGAYN (Y=C/U, N=U/A/C/G), AAACK (K=G/U) and NBNAH (N=U/A/C/G, B=G/C/U, H=C/U/A), RAACW (R=G/A, W=U/A). These motifs closely resemble the well-known m^{6}A binding motif, RRACH (R=G/A, H=A/C/U).

Further we asked which RNA molecules prefer to contain m^{6}A modification. We assigned confident m^{6}A peaks to GRCh38 genome and found that 76.24% and 77.78% were mRNA, 18.42% and 17.16% were long non-coding RNA (lncRNA) in normal and chRCC tissues (Fig. 2D), separately. We also noticed that the confident m^{6}A peaks number in chRCC tissues were less than that in normal tissues. Then we assigned m^{6}A peaks to chromosome, genes and five non-overlapping regions. We found that the number of confident m^{6}A peaks in chRCC tissues

decreased globally among each chromosome (Fig. 2E). By analyzing the distribution of m^{6}A peaks per gene, we found that most of m^{6}A-motified mRNAs contained one or two m^{6}A peak, while a small number of them contained three or more (Fig. 2F). Furthermore, m^{6}A number per gene in chRCC tissues was all less than that in normal tissues. We also counted the number of m^{6}A peaks among the five non-overlapping regions in normal and chRCC tissues (Fig. 2G) and found the number of m^{6}A peaks decreased in chRCC tissues (except start codon) too. These results suggested that m^{6}A modification level decreased in cancer tissues.

Differentially methylated m^{6}A genes (DMMGs) participate in multi-cancer related pathways

To dissect the role of m^{6}A modification, we subsequently identified DMMPs between normal and chRCC tissues. Compared to the normal tissues, the hyper- and hypo-methylated peaks were respectively regarded as hyper and hypo group. As to hyper group, we identified 644 shared differentially hyper-methylated m^{6}A peaks corresponding to 593 genes in the three biological replicates. While as to hypo group, we identified 1304 shared differentially hypo-methylated m^{6}A peaks representing 1137 genes (Fig. 3A). We further identified the m^{6}A motif in hyper- and hypo- methylated m^{6}A peaks within chRCC

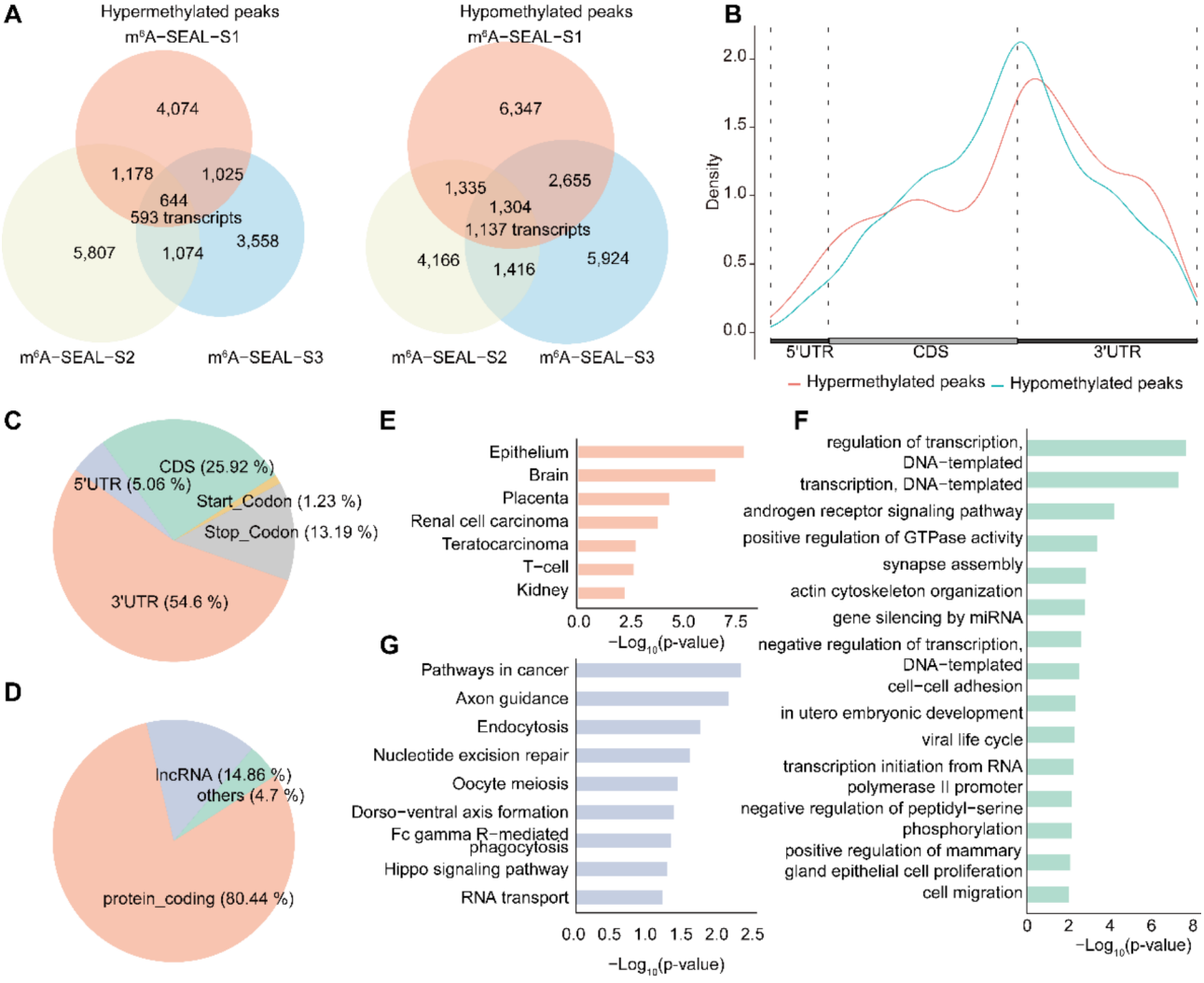

Fig. 3 Tissue analysis, Gene Ontology (GO) and Kyoto Encyclopedia of Genes and Genomes (KEGG) analyses of coding genes containing hypomethylation m^{6}A peaks in chRCC tissues. **A**, Overlap of three biological replicates of hypermethylation m^{6}A peaks identifying ~ 644 high-confident hypermethylation m^{6}A peaks corresponding to 593 unique transcripts in chRCC tissues (left); Overlap of three biological replicates of hypomethylation m^{6}A peaks identifying ~ 1,304 high-confident hypomethylation m^{6}A peaks corresponding to 1,137 unique transcripts in chRCC tissues (right). **B**, Metagene profile illustrating the region distribution of hypermethylation and hypomethylation m^{6}A peaks across the indicated mRNA segments. **C**, Pie chart presenting the fraction of the confident hypomethylation m^{6}A peaks five non-overlapping transcript segments; **D**, Pie chart presenting RNA types (that is, transcript species) of the confident hypomethylation m^{6}A peaks identified in chRCC. **E**-**G**, UP_TISSUE (**E**), Gene ontology (GO) (**F**), KEGG (**G**) analysis of the confident hypomethylation m^{6}A genes

tissues by HOMER, and it revealed that the top consensus motifs in the hyper- and hypo-methylated m^{6}A peaks were both similar to RRACH (Fig. S4).

Then we examined the distribution profiles of DMMPs across the transcripts, and found that the density of DMMPs tended to be around the stop codon in both hyper and hypo group. In hypo group, the m^{6}A peaks were especially enriched in the CDS and 3' UTR near the stop codon; whereas in the hyper group, m^{6}A peaks were enriched in the 3' UTR near the stop codon (Fig. 3B). Further examination revealed that the m^{6}A peaks in both groups were dominantly enriched within 3′ UTR (54.6% and 56.68%), CDS (25.92% and 23.14%) and around stop codon (13.19% and 11.02%) (Fig. 3C and Fig. S3A). Almost all of the transcripts containing DMMPs were mRNA (80.44% and 70.61%), only ~ 14–18% were lncRNA and a small proportion were other RNAs (Fig. 3D and Fig. S3B).

To explore the potential role of hypo-methylated m^{6}A peaks in chRCC, we took advantage of DAVID to examine the most preferential expression tissues of genes with hypo-methylated peaks. The results showed that genes containing hypo-methylated m^{6}A sites preferentially expressed in epithelium, followed by brain, placenta and renal cell carcinoma (RCC) (Fig. 3E), indicating the correlation between these genes and RCC. Furthermore, we performed GO enrichment analysis to uncover the functions of these genes. The results revealed that genes with hypo-methylated m^{6}A peaks were enriched in many biological processes involved in kidney development and cancer pathogenesis, including transcription, androgen receptor signaling pathway, GTPase activity and cell-cell adhesion (Fig. 3F). Pathway analysis showed that genes with hypo-methylated m^{6}A peaks were mainly enriched in pathways in cancer (Fig. 3G). These results suggested that genes with hypo-methylated peaks may participate in various pathophysiologic aspects of kidney cancer through different pathways.

Subsequently, we explored the potential function of hyper-methylated m^{6}A peaks using the same method. The results showed that genes containing hyper-methylated m^{6}A sites preferentially expressed in brain, followed by epithelium, duodenum, fetal kidney and ovary (Fig. S3C) which also indicating these genes is important in kidney development. GO biological process analysis revealed that genes with hyper-methylated m^{6}A peaks were significantly associated with cancer-related biological processes, including protein phosphorylation, positive regulation of cholesterol efflux, ubiquinone biosynthetic process, regulation of mitophagy and so on (Fig. S3D). Pathway analysis showed that genes with hyper-methylated m^{6}A peaks were mainly enriched in ubiquitin mediated proteolysis, metabolic pathways and adherents' junction (Fig. S3E). These results further illustrated that gene with DMMPs played crucial roles in kidney cancer.

Differentially expressed genes involved in kidney development and cancer occurrence

We next identified the global mRNA expression patterns in normal and cancer groups. The results showed that a total of 3,911 mRNAs were significantly dysregulated in cancer group compared with normal group, including 2,344 down-regulated mRNAs and 1,567 up-regulated mRNAs (fold change ≥ 2, $P < 0.05$) (Fig. 4A). Hierarchical clustering depicted differential expression profiles in all the samples. (Fig. 4B). We then took advantage of the DAVID to examine the preferentially expressed tissues of these genes. The results showed that the dysregulated genes preferentially expressed in kidney, followed by liver and plasma (Fig. 4C). Then we performed GO analysis and KEGG pathway analysis. GO enrichment analysis demonstrated that dysregulated genes were significantly enriched in kidney development and cancer related biological processes involving metabolic process, cell adhesion and kidney development (Fig. 4D). While the KEGG pathway analysis revealed that dysregulated genes were significantly associated with metabolic pathways and protein metabolism (Fig. 4E).

Novel m^{6}A gene signature identified by m^{6}A-SEAL-seq and RNA-seq data

We comprehensively analyzed m^{6}A-SEAL-seq and RNA-seq data in normal and chRCC tissues. The results demonstrated that among the 593 hyper-methylated genes detected by m^{6}A-SEAL-seq, 44 targets tended to be down-regulated and 68 targets tended to be up-regulated (Fig. 5A, left); among the 1,137 hypo-methylated genes, 123 targets tended to be down-regulated and 51 targets tended to be up-regulated (Fig. 5A, right). Further, a significant increase of RPKM was observed in the hyper group compared to the hypo group (Fig. 5B).

To further analyze the role of DMMGs in cancers, we intersected DMMGs with Cancer Gene Census (CGC) database [49], a database consists of genes with strong indications of a role in cancer, and found 73 and 23 genes were annotated in hypo-methylated and hyper-methylated genes separately (Supplementary Dataset 3 and 4). Among these cancer related genes, 10 genes were differentially expressed genes, including NOCH1 and FGFR1. According to Integrative Genomics Viewer (IGV) software, the m^{6}A modification level of NOTCH1 decreased significantly (Fig. 5C, left), then we measure the expression level of NOTCH1 and found in chRCC tissue, the expression level of NOTCH1 reduced significantly (Fig. 5C, right), suggesting NOTCH1 acts as a tumor suppressor gene in chRCC. Fibroblast growth factor receptor 1 (FGFR1) is a well-known oncogene. We found the

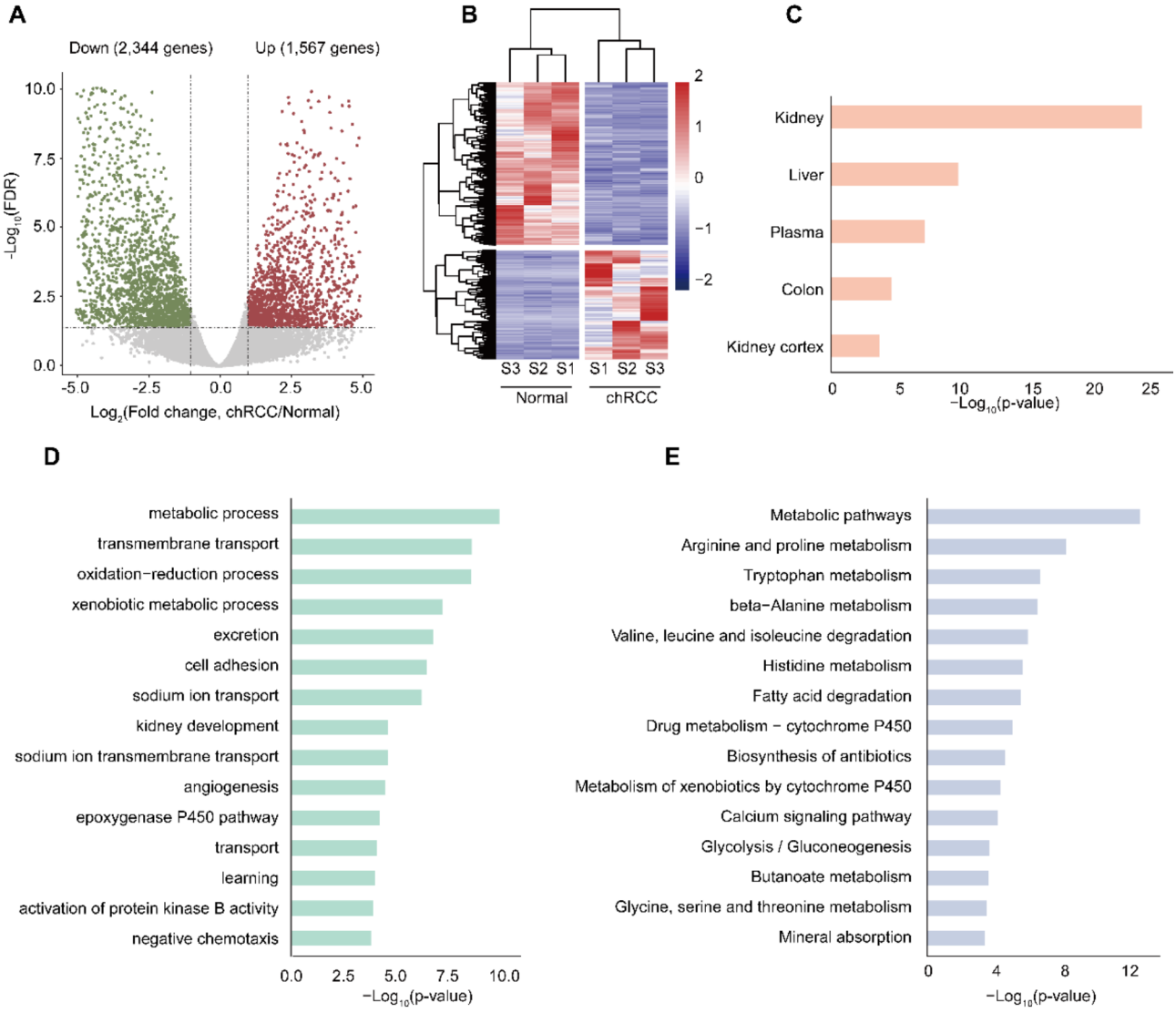

Fig. 4 Differential expression genes in chRCC tissues compared with adjacent normal tissues. **A**, Volcano plots showing the differentially expressed genes in chRCC tissues compared with those in adjacent normal tissues. **B**, Heatmap plots showing the differentially expressed genes in chRCC tissues vs. those in adjacent normal tissues. C-E, UP_TISSUE (**C**), Gene ontology (GO) (**D**), KEGG (**E**) analysis of the differential expression genes

m^{6}A modification level of FGFR1 decreased significantly (Fig. 5D, left) and the expression level of FGFR1 increased in chRCC tissue (Fig. 5D, right). We observed differences in the expression patterns of these two genes, with both showing hyper-methylation in their modification levels but opposite expression patterns. This discrepancy indicates potential differences in m^{6}A regulation pathways.

Thus, we conducted principal component analysis of the differential expressed DMMGs in 65 chRCC cases from The Cancer Genome Atlas (TCGA) database. Based on the expression of these genes, we could completely distinguish chRCC samples from normal samples (Fig. 5E). Cox regression screen and least absolute shrinkage and selection operator (LASSO) identified three m^{6}A-dependent signatures (Supplementary Dataset 5) and defined a m^{6}A-dependent cox model in the training set (Fig. S5A). Concordance index (C-index=0.96) showed that the proposed model has a high prognostic power. In this model, we separated patients into high-risk or low-risk group according to their risk score, and patients with different 5-years survival could be distinguished completely between the two groups (Log-rank $p<0.0001$) (Fig. 5F). AUC of ROC curve also confirmed the prognostic power of the m^{6}A-dependent model (Fig. S5B). Then the proposed model was applied to the testing set for prediction. We calculated risk score of each patient in the testing set and assigned to high-risk or low-risk group according to the cut off value in the training set. The Kaplan-Meier survival curve and log-rank between the two groups showed significant difference

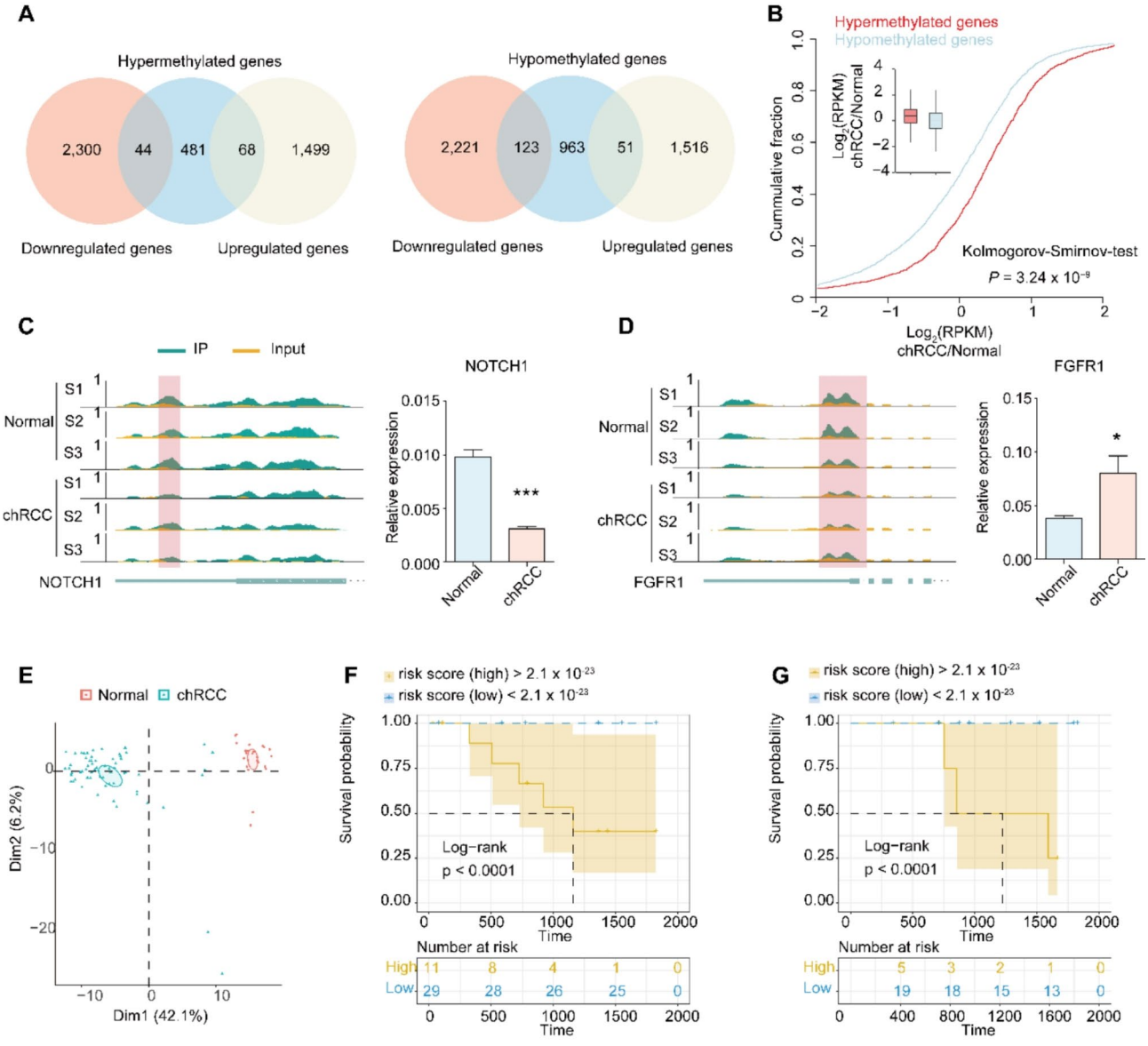

Fig. 5 Conjoint analysis of m^{6}A-SEAL-seq and RNA-seq data. **A**, Overlap of hypermethylation genes with up-regulation genes and down-regulation genes (left). Overlap of hypomethylation genes with up-regulation genes and down-regulation genes (right). **B**, Cumulative distribution displaying the expression level changes in mRNAs with hypermethylation or hypomethylation m^{6}A modification. C-D, Integrative genomics viewer (IGV) tracks showing the indicated m^{6}A-seal reads distribution on target transcripts and the relative expression level in Normal and chRCC tissues. (**C**) NOTCH1, (**D**) FGFR1. **F**-**G** Survival analyses in the training set (**F**) and testing set (**G**). Log-rank $p < 0.0001$ showed a significant survival difference between the two sub-groups

(Fig. 5G), which demonstrated the high predictive ability of the m^{6}A-dependent model. Furthermore, we also test the m^{6}A-dependent model in ccRCC samples (a cohort of 602 cases from TCGA database) and PRCC dataset (a cohort of 318 cases from TCGA database). The results indicated that the m^{6}A-dependent model is also suitable for ccRCC, but not PRCC (Fig. S5C, D).

Discussion

Despite having the lowest incidence and mortality rates among the three main types of kidney cancer, chRCC still contributes to thousands of deaths worldwide, according to statistics from the GCO in 2022. Over the past few years, there has been a growing effort to elucidate the mechanism of m^{6}A modification in RCC, resulting in extensive accumulation of knowledge regarding the correlation between m^{6}A modification and RCC. However, chRCC has been overlooked. Here, we demonstrated that m^{6}A writer WTAP and m^{6}A erasers FTO and ALKBH5 were downregulated in chRCC tissues, which may result in a different m^{6}A modification pattern in chRCC tissues. By m^{6}A-SEAL-seq, we confirmed that m^{6}A modification pattern in chRCC tissues is distinct from that in normal tissues. The m^{6}A peaks number and m^{6}A peaks per

gene in chRCC decreased and the distribution pattern of m^6A peaks shifted to 3'UTR orientation in chRCC. Further functional studies showed that genes with hyper- or hypo-methylated peaks were mainly enriched in kidney development and cancer pathogenesis related pathway, which is a further proof of the fundamental role of m^6A modification in chRCC. We also found m^6A reader YTHDF2 were downregulated in chRCC tissues. The role of YTHDF2 in m^6A-dependent gene regulation, particularly its impact on RNA stability, suggests the existence of m^6A-dependent RNA degradation and gene dysregulation in chRCC. The down-regulation of NOTCH1 may be attributed to the down-regulation of YTHDF2. Additionally, the observed discrepancy in the expression pattern of FGFR1 indicates potential differences in m^6A regulation pathways. Cumulative fraction of genes with hyper-methylated peaks and genes with hypo-methylated peaks indicated that these two group gene sets have different expression pattern in chRCC tissues, which may result from the dysregulation of m^6A readers, such as YTHDF2.

In the present study, we depicted transcriptome-wide m^6A profiling in normal and chRCC tissues by an antibody-free method. By comparing the m^6A peaks in normal tissues and chRCC tissues, we revealed a total of 1730 DMMGs including 593 hyper- and 1137 hypo-methylated genes in chRCC tissues, which may be important factors in chRCC. For example, RARA, one of the hypo-methylated genes, has been demonstrated as a target of FTO in acute myeloid leukemia (AML). The m^6A on *RARA* at UTRs influences the stability of *RARA*. The decreased m^6A modification level of *RARA* destabilizes *RARA* mRNA, and then promotes tumorigenesis [50]. By CGC database analysis [49], we found 96 genes were causally implicated in cancers, such as ZEB1, which acts as an oncogene in ccRCC, PBRM1, ASXL2 and SETD2, which act as tumor suppressor genes in ccRCC. These results indicate m^6A modification has a major influence on ccRCC, implying the roles of m^6A modification in chRCC. Combined with our RNAseq data, we found 10 genes were differential expressed genes, including *NOTCH1* and *FGFR1*. The level of m^6A on NOTCH1 at 3'UTR and the expression level of *NOTCH1* reduced significantly, which are similar to *PER1* in pancreatic cancer and *RARA* in AML [33, 50]. *PER1*'s degradation is YTHDF2-dependent manner, while the mechanism underlying the degradation of *NOTCH1* and *RARA* remains unknown. The level of m^6A on *FGFR1* at 3'UTR also decreased, but the expression level of *FGFR1* increased significantly. It is reported that m^6A reader IGF2BP3 enhances mRNA stability in an m^6A-dependent manner [13, 51], which may account for the upregulation of FGFR1 in chRCC. Further functional studies are needed to clarify the molecular mechanisms of above-mentioned genes in the development of chRCC.

Despite the insights gained from our study, it is important to acknowledge a significant limitation: the small sample size. Our findings are based on data obtained from only three chRCC patients, which may not be sufficient to draw definitive conclusions about m^6A modifications in chRCC. While the observed patterns in m^6A regulation provide valuable initial insights, larger cohorts are needed to validate these results and ensure that they are broadly applicable to the wider chRCC patient population. Future studies with expanded sample sizes will be essential for confirming the role of m^6A modifications in chRCC and for elucidating the underlying mechanisms with greater accuracy.

Supplementary Information

The online version contains supplementary material available at https://doi.org/10.1186/s12885-024-12956-6.

Supplementary Material 1

Supplementary Material 2

Author contributions

The project was conceptualized and designed by Baoguo Li, Lulin Ma and Guifang Jia. Experiments were conducted by Zhigang Chen, Wei Zhang, Yang Qian, Nan Zhang，Min Lu, Liyuan Ge, Cheng Liu and Xiaojun Tian. The sequencing data were analyzed by Junbo Yang and Zixin Chen. Zhigang Chen, Junbo Yang and Wei Zhang wrote the manuscript. Baoguo Li, Lulin Ma and Guifang Jia revised the manuscript. All authors reviewed the manuscript and attest that they meet the current ICMJE criteria for authorship.

Funding

This work was supported by the National Basic Research Program of China (2019YFA0802201 and 2017YFA0505201), Beijing Natural Science Foundation (Z200010) and Beijing Haidian Hospital research fund (KYQ 2022018).

Data availability

The raw sequence data of RNA-seq (input), m^6A-SEAL-seq have been deposited in the Genome Sequence Archive in the National Genomics Data Center (NGDC), Beijing Institute of Genomics, Chinese Academy of Sciences, under accession number (PRJCA004912).

Declarations

Ethical approval

Our research was conducted in accordance with the principles of the Declaration of Helsinki. The study was approved by The Beijing Haidian Hospital Medical Ethics Committee under the Project number M202231 and approval number 2022 – 112. Written informed consent was obtained from all participants prior to collecting clinical specimens for research purposes. All specimens were stored securely and handled using appropriate procedures to maintain their integrity. De-identified data were used in all analyses to protect patient privacy.

Competing interests

The authors declare no competing interests.

Received: 25 April 2024 / Accepted: 17 September 2024
Published online: 27 September 2024

References

1. Jonasch E, Walker CL, Rathmell WK. Clear cell renal cell carcinoma ontogeny and mechanisms of lethality. Nat Rev Nephrol. 2021;17:245–61.

2. Martínez-Sáez O, Gajate Borau P, Alonso-Gordoa T, Molina-Cerrillo J, Grande E. Targeting HIF-2 α in clear cell renal cell carcinoma: a promising therapeutic strategy. Crit Rev Oncol Hematol. 2017;111:117–23.
3. Atkins MB, Tannir NM. Current and emerging therapies for first-line treatment of metastatic clear cell renal cell carcinoma. Cancer Treat Rev. 2018;70:127–37.
4. Wolf MM, Kimryn Rathmell W, Beckermann KE. Modeling clear cell renal cell carcinoma and therapeutic implications. Oncogene. 2020;39:3413–26.
5. McCroskey Z, Sim SJ, Selzman AA, Ayala AG, Ro JY. Primary collision tumors of the kidney composed of oncocytoma and papillary renal cell carcinoma: a review. Ann Diagn Pathol. 2017;29:32–6.
6. Rogala J, Kojima F, Alaghehbandan R, Agaimy A, Martinek P, Ondic O, Ulamec M, Sperga M, Michalova K, Pivovarcikova K, Pitra T, Hora M, Ferak I, Marečková J, Michal M, Hes O. Papillary renal cell carcinoma with prominent spindle cell stroma - tumor mimicking mixed epithelial and stromal tumor of the kidney: clinicopathologic, morphologic, immunohistochemical and molecular genetic analysis of 6 cases. Ann Diagn Pathol. 2020;44:151441.
7. Moch H, Cubilla AL, Humphrey PA, Reuter VE, Ulbright TM. The 2016 WHO classification of Tumours of the urinary system and male genital organs-Part A: renal, Penile, and testicular tumours. Eur Urol. 2016;70:93–105.
8. Przybycin CG, Cronin AM, Darvishian F, Gopalan A, Al-Ahmadie HA, Fine SW, Chen YB, Bernstein M, Russo P, Reuter VE, Tickoo SK. Chromophobe renal cell carcinoma: a clinicopathologic study of 203 tumors in 200 patients with primary resection at a single institution. Am J Surg Pathol. 2011;35:962–70.
9. Davis CF, Ricketts CJ, Wang M, Yang L, Cherniack AD, Shen H, Buhay C, Kang H, Kim SC, Fahey CC, Hacker KE, Bhanot G, Gordenin DA, Chu A, Gunaratne PH, Biehl M, Seth S, Kaipparettu BA, Bristow CA, Donehower LA, Wallen EM, Smith AB, Tickoo SK, Tamboli P, Reuter V, Schmidt LS, Hsieh JJ, Choueiri TK, Hakimi AA, Chin L, Meyerson M, Kucherlapati R, Park WY, Robertson AG, Laird PW, Henske EP, Kwiatkowski DJ, Park PJ, Morgan M, Shuch B, Muzny D, Wheeler DA, Linehan WM, Gibbs RA, Rathmell WK. C.J. Creighton, The somatic genomic landscape of chromophobe renal cell carcinoma, Cancer Cell, 26 (2014) 319–330.
10. Cantara WA, Crain PF, Rozenski J, McCloskey JA, Harris KA, Zhang X, Vendeix FA, Fabris D, Agris PF. The RNA modification database, RNAMDB: 2011 update. Nucleic Acids Res. 2011;39:D195–201.
11. Wang X, Lu Z, Gomez A, Hon GC, Yue Y, Han D, Fu Y, Parisien M, Dai Q, Jia G, Ren B, Pan T, He C. N6-methyladenosine-dependent regulation of messenger RNA stability. Nature. 2014;505:117–20.
12. Wei LH, Song P, Wang Y, Lu Z, Tang Q, Yu Q, Xiao Y, Zhang X, Duan HC, Jia G. The m(6)a reader ECT2 controls Trichome morphology by affecting mRNA Stability in Arabidopsis. Plant Cell. 2018;30:968–85.
13. Huang H, Weng H, Sun W, Qin X, Shi H, Wu H, Zhao BS, Mesquita A, Liu C, Yuan CL, Hu YC, Hüttelmaier S, Skibbe JR, Su R, Deng X, Dong L, Sun M, Li C, Nachtergaele S, Wang Y, Hu C, Ferchen K, Greis KD, Jiang X, Wei M, Qu L, Guan JL, He C, Yang J, Chen J. Recognition of RNA N(6)-methyladenosine by IGF2BP proteins enhances mRNA stability and translation. Nat Cell Biol. 2018;20:285–95.
14. Hou Y, Sun J, Wu B, Gao Y, Nie H, Nie Z, Quan S, Wang Y, Cao X, Li S. CPSF30-L-mediated recognition of mRNA m(6)a modification controls alternative polyadenylation of nitrate signaling-related gene transcripts in Arabidopsis. Mol Plant. 2021;14:688–99.
15. Song P, Yang J, Wang C, Lu Q, Shi L, Tayier S, Jia G. Arabidopsis N(6)-methyladenosine reader CPSF30-L recognizes FUE signals to control polyadenylation site choice in liquid-like nuclear bodies. Mol Plant. 2021;14:571–87.
16. Horiuchi K, Kawamura T, Iwanari H, Ohashi R, Naito M, Kodama T, Hamakubo T. Identification of Wilms' tumor 1-associating protein complex and its role in alternative splicing and the cell cycle. J Biol Chem. 2013;288:33292–302.
17. Xiao W, Adhikari S, Dahal U, Chen YS, Hao YJ, Sun BF, Sun HY, Li A, Ping XL, Lai WY, Wang X, Ma HL, Huang CM, Yang Y, Huang N, Jiang GB, Wang HL, Zhou Q, Wang XJ, Zhao YL, Yang YG. Nuclear m(6)a reader YTHDC1 regulates mRNA splicing. Mol Cell. 2016;61:507–19.
18. Barbieri I, Tzelepis K, Pandolfini L, Shi J, Millán-Zambrano G, Robson SC, Aspris D, Migliori V, Bannister AJ, Han N, De Braekeleer E, Ponstingl H, Hendrick A, Vakoc CR, Vassiliou GS, Kouzarides T. Promoter-bound METTL3 maintains myeloid leukaemia by m(6)A-dependent translation control. Nature. 2017;552:126–31.
19. Wang X, Zhao BS, Roundtree IA, Lu Z, Han D, Ma H, Weng X, Chen K, Shi H, He C, 6 N, Modulates methyladenosine, RNA M, Efficiency T. Cell. 2015;161:1388–99.
20. Bokar JA, Shambaugh ME, Polayes D, Matera AG, Rottman FM. Purification and cDNA cloning of the AdoMet-binding subunit of the human mRNA (N6-adenosine)-methyltransferase. RNA. 1997;3:1233–47.
21. Liu J, Yue Y, Han D, Wang X, Fu Y, Zhang L, Jia G, Yu M, Lu Z, Deng X, Dai Q, Chen W, He C. A METTL3-METTL14 complex mediates mammalian nuclear RNA N6-adenosine methylation. Nat Chem Biol. 2014;10:93–5.
22. Yang Y, Hsu PJ, Chen YS, Yang YG. Dynamic transcriptomic m(6)a decoration: writers, erasers, readers and functions in RNA metabolism. Cell Res. 2018;28:616–24.
23. Ping XL, Sun BF, Wang L, Xiao W, Yang X, Wang WJ, Adhikari S, Shi Y, Lv Y, Chen YS, Zhao X, Li A, Yang Y, Dahal U, Lou XM, Liu X, Huang J, Yuan WP, Zhu XF, Cheng T, Zhao YL, Wang X, Rendtlew Danielsen JM, Liu F, Yang YG. Mammalian WTAP is a regulatory subunit of the RNA N6-methyladenosine methyltransferase. Cell Res. 2014;24:177–89.
24. Agarwala SD, Blitzblau HG, Hochwagen A, Fink GR. RNA methylation by the MIS complex regulates a cell fate decision in yeast. PLoS Genet. 2012;8:e1002732.
25. Jia G, Fu Y, Zhao X, Dai Q, Zheng G, Yang Y, Yi C, Lindahl T, Pan T, Yang YG, He C. N6-methyladenosine in nuclear RNA is a major substrate of the obesity-associated FTO. Nat Chem Biol. 2011;7:885–7.
26. Zheng G, Dahl JA, Niu Y, Fedorcsak P, Huang CM, Li CJ, Vågbø CB, Shi Y, Wang WL, Song SH, Lu Z, Bosmans RP, Dai Q, Hao YJ, Yang X, Zhao WM, Tong WM, Wang XJ, Bogdan F, Furu K, Fu Y, Jia G, Zhao X, Liu J, Krokan HE, Klungland A, Yang YG, He C. ALKBH5 is a mammalian RNA demethylase that impacts RNA metabolism and mouse fertility. Mol Cell. 2013;49:18–29.
27. Zhang Z, Theler D, Kaminska KH, Hiller M, de la Grange P, Pudimat R, Rafalska I, Heinrich B, Bujnicki JM, Allain FH, Stamm S. The YTH domain is a novel RNA binding domain. J Biol Chem. 2010;285:14701–10.
28. Xu C, Wang X, Liu K, Roundtree IA, Tempel W, Li Y, Lu Z, He C, Min J. Structural basis for selective binding of m^{6}A RNA by the YTHDC1 YTH domain. Nat Chem Biol. 2014;10:927–9.
29. Li F, Zhao D, Wu J, Shi Y. Structure of the YTH domain of human YTHDF2 in complex with an m(6)a mononucleotide reveals an aromatic cage for m(6)a recognition. Cell Res. 2014;24:1490–2.
30. Liu T, Wei Q, Jin J, Luo Q, Liu Y, Yang Y, Cheng C, Li L, Pi J, Si Y, Xiao H, Li L, Rao S, Wang F, Yu J, Yu J, Zou D, Yi P. The m^{6}A reader YTHDF1 promotes ovarian cancer progression via augmenting EIF3C translation. Nucleic Acids Res. 2020;48:3816–31.
31. Chen Y, Peng C, Chen J, Chen D, Yang B, He B, Hu W, Zhang Y, Liu H, Dai L, Xie H, Zhou L, Wu J, Zheng S. WTAP facilitates progression of hepatocellular carcinoma via m^{6}A-HuR-dependent epigenetic silencing of ETS1. Mol Cancer. 2019;18:127.
32. He L, Li H, Wu A, Peng Y, Shu G, Yin G. Functions of N6-methyladenosine and its role in cancer. Mol Cancer. 2019;18:176.
33. Guo X, Li K, Jiang W, Hu Y, Xiao W, Huang Y, Feng Y, Pan Q, Wan R. RNA demethylase ALKBH5 prevents pancreatic cancer progression by posttranscriptional activation of PER1 in an m^{6}A-YTHDF2-dependent manner. Mol Cancer. 2020;19:91.
34. Han J, Wang JZ, Yang X, Yu H, Zhou R, Lu HC, Yuan WB, Lu JC, Zhou ZJ, Lu Q, Wei JF, Yang H. METTL3 promote tumor proliferation of bladder cancer by accelerating pri-miR221/222 maturation in m^{6}A-dependent manner. Mol Cancer. 2019;18:110.
35. Chen S, Zhang N, Zhang E, Wang T, Jiang L, Wang X, Zheng J. A novel m(6)a gene signature Associated with Regulatory Immune function for Prognosis Prediction in Clear-Cell Renal Cell Carcinoma. Front Cell Dev Biol. 2020;8:616972.
36. Wang Q, Zhang H, Chen Q, Wan Z, Gao X, Qian W. Identification of METTL14 in Kidney Renal Clear Cell Carcinoma Using Bioinformatics Analysis, Dis Markers, 2019 (2019) 5648783.
37. Zhou J, Wang J, Hong B, Ma K, Xie H, Li L, Zhang K, Zhou B, Cai L, Gong K. Gene signatures and prognostic values of m^{6}A regulators in clear cell renal cell carcinoma - a retrospective study using TCGA database. Aging. 2019;11:1633–47.
38. Sun Z, Jing C, Xiao C, Li T, Wang Y. Prognostic risk signature based on the expression of three m^{6}A RNA methylation regulatory genes in kidney renal papillary cell carcinoma. Aging. 2020;12:22078–94.
39. Chen Y, Zhou C, Sun Y, He X, Xue D. M(6)a RNA modification modulates gene expression and cancer-related pathways in clear cell renal cell carcinoma. Epigenomics. 2020;12:87–99.
40. Wang Y, Xiao Y, Dong S, Yu Q, Jia G. Antibody-free enzyme-assisted chemical approach for detection of N(6)-methyladenosine. Nat Chem Biol. 2020;16:896–903.
41. Xia H, Zhang Z, Luo C, Wei K, Li X, Mu X, Duan M, Zhu C, Jin L, He X, Tang L, Hu L, Guan Y, Lam DCC, Yang J. MultiPrime: A reliable and efficient tool for targeted next-generation sequencing, iMeta, n/a e143.

42. Martin M. CUTADAPT removes adapter sequences from high-throughput sequencing reads. EMBnet J, 17 (2011).
43. Pertea M, Kim D, Pertea GM, Leek JT, Salzberg SL. Transcript-level expression analysis of RNA-seq experiments with HISAT, StringTie and Ballgown. Nat Protoc. 2016;11:1650–67.
44. Zhang Y, Liu T, Meyer CA, Eeckhoute J, Johnson DS, Bernstein BE, Nusbaum C, Myers RM, Brown M, Li W, Liu XS. Model-based analysis of ChIP-Seq (MACS). Genome Biol. 2008;9:R137.
45. Heinz S, Benner C, Spann N, Bertolino E, Lin YC, Laslo P, Cheng JX, Murre C, Singh H, Glass CK. Simple combinations of lineage-determining transcription factors prime cis-regulatory elements required for macrophage and B cell identities. Mol Cell. 2010;38:576–89.
46. Cui X, Zhang L, Meng J, Rao MK, Chen Y, Huang Y. MeTDiff: a Novel Differential RNA methylation analysis for MeRIP-Seq Data. IEEE/ACM Trans Comput Biol Bioinform. 2018;15:526–34.
47. Love MI, Huber W, Anders S. Moderated estimation of Fold change and dispersion for RNA-seq data with DESeq2. Genome Biol. 2014;15:550.
48. Zhang H, Shi X, Huang T, Zhao X, Chen W, Gu N, Zhang R. Dynamic landscape and evolution of m^6A methylation in human. Nucleic Acids Res. 2020;48:6251–64.
49. Sondka Z, Bamford S, Cole CG, Ward SA, Dunham I, Forbes SA. The COSMIC Cancer Gene Census: describing genetic dysfunction across all human cancers. Nat Rev Cancer. 2018;18:696–705.
50. Li Z, Weng H, Su R, Weng X, Zuo Z, Li C, Huang H, Nachtergaele S, Dong L, Hu C, Qin X, Tang L, Wang Y, Hong GM, Huang H, Wang X, Chen P, Gurbuxani S, Arnovitz S, Li Y, Li S, Strong J, Neilly MB, Larson RA, Jiang X, Zhang P, Jin J, He C, Chen J. FTO plays an oncogenic role in Acute myeloid leukemia as a N(6)-Methyladenosine RNA demethylase. Cancer Cell. 2017;31:127–41.
51. Gu Y, Niu S, Wang Y, Duan L, Pan Y, Tong Z, Zhang X, Yang Z, Peng B, Wang X, Han X, Li Y, Cheng T, Liu Y, Shang L, Liu T, Yang X, Sun M, Jiang S, Zhang C, Zhang N, Ye Q, Gao S. DMDRMR-Mediated regulation of m(6)A-Modified CDK4 by m(6)a reader IGF2BP3 drives ccRCC progression. Cancer Res. 2021;81:923–34.

Publisher's note

Springer Nature remains neutral with regard to jurisdictional claims in published maps and institutional affiliations.